RSC Advances

ROYAL SOCIETY OF CHEMISTRY

www.rsc.org/advances

Sensitivity of Coalescence Separation of Oil-Water Emulsions Using Stainless Steel Felt Enabled by LBL Self-Assembly and CVD

Xiaoyu Li[a], Dan Hu[a,b], Lixia Cao[a] and Chuanfang Yang[a,*]

[a]*Key Laboratory of Green Process and Engineering, National Key Laboratory of Biochemical Engineering, Institute of Process Engineering, Chinese Academy of Sciences, Beijing 100190, China*

[b]*University of Chinese Academy of Sciences, Beijing 100049, China*

** Corresponding author.*

Tel/Fax: +86 10 82544976. E-mail: cfyang@ipe.ac.cn

Electronic supplementary information (ESI) available: Fig. S1-S10 and Movies.

Abstract: Commercial stainless steel felt was endowed by LBL self-assembly of dual size nano-SiO_2 particles to have hierarchical micro/nano surface structure. The pore size of the felt was tailored at the same time by tuning the assembling cycles. Chemical vapor deposition (CVD) of 1H, 1H, 2H, 2H-perfluorooctyltriethoxysilane (POTS) at two concentration levels was applied to the roughened felt to render it both hydrophobic/superhydrophobic and oleophobic. The felt thus prepared was wettable by oil underwater, which allowed it to be effective as a coalescing material for separating 4 kinds of oil-in-water emulsions. The nanometer-thick POTS coating was durable for months. The coalescence separation efficiency was found to be dependent on both pore size and surface wettability of the felt in air. It was less sensitive to pore

size change when the surface was more hydrophobic and oleophobic (amphiphobic). When pore size was kept constant, more amphiphobic felt was less efficient for separation. When the surface turned superhydrophobic, the separation became better as pore size was reduced. These findings provide new insights for designing better coalescence materials, especially when the effects of surface wettability and pore size are intermingled.

1. Introduction

Oil-water separation has attracted considerable attention because of tightened environmental regulations and the needs of water recycle and reuse. Compared with the separation of common oil-water mixtures, effective separation of emulsified oil in wastewater is much more challenging due to the emulsion's stability.[1-4] Conventional techniques for oil-water separation include gravity, skimming, flocculation, air flotation, coalescence and oil absorbing. However, these techniques are often limited in practical applications by either high energy-cost, secondary environmental pollution, or complex separation instruments required and low separation efficiencies, especially for tiny oil droplets.[2,4-7] Recently, gravity-driven oil-water separation becomes attractive due to its self-driven flow without the need of applying external power.[8-14] For example, Wang et al. reported that a mesh with self-cleaning and underwater superoleophobicity could be used for gasoline-water separation.[9] Lin's group reported that a smart hydrogel coated mesh, when triggered by thermo and pH, could selectively separate water from oil/water mixtures.[14] Interestingly, these work

and their likes, relied on sieving mechanism and surface oleophobicity or superoleophobicity for separation. They also focused mainly on the removal of large oil droplets from common and unstable oil-water mixtures instead of relatively stable and tiny oil-in-water emulsions. Membrane separation, although vulnerable to fouling, is also attractive for oil contaminated water treatment because of the small membrane pore size and the designed surface oleophobicity required for such separations.[15] For example, some membrane-oriented technologies were recently demonstrated to be able to achieve energy-saving, easy and efficient separation of emulsified oil-water mixtures.[16-22] However, these techniques are still in exploratory stage, further investigation and development such as the selection of suitable membranes and membrane modification methods, are therefore needed to prove their worth for difficult applications.[23-26]

Inspired by lotus leaf, rose petal, strider leg, and so on, scientists realized that the regulation of micro- and nano-scale hierarchical structure and surface energy toward the object surface can achieve super wettability (superhydrophilicity, superhydrophobicity, superoleophilicity, underwater superoleophobicity, and superamphiphobicity, etc).[27-32] Such ideas have been employed to prepare materials for oil-water separation by sieving,[33-47] and most reported methods centered on modifying two-dimensional (2D) surfaces of porous meshes or textiles to achieve super wettability.[35-39] Another approach to achieving oil-water separation relies on absorption/adsorption by employing 3D bulk materials such as foams or sponges modified to possess super wettability.[40-44] Again, most materials were used to separate

only common, unstable oil-water mixtures that could also be delivered with alternative methods relatively easily.[45-48] There were exceptions, however, which targeted the more challenging separation of oil-water emulsions. For example, Tuteja's group reported that a constructed film with both superhydrophilicity and superoleophobicity, in air and under water, could effectively separate water-in-oil emulsions.[8] We reported recently that by constructing a rough hydrophobic and oleophobic surface on stainless steel felt, oil-in-water emulsion of 2 μm could be efficiently separated by using the felt as a coalescence material.[49] Coalescence process allows the emulsion to pass through the material where the dispersed phase is captured and enlarged inside the material, released and separated by gravitational/buoyancy force downstream outside the material (Figure S1 in Supporting Information). It is an opposite process to membrane pore sieving separation that relies on the relative smaller pore size to droplet size as well as surface repellency to separate the droplets. Good separation can still be accomplished using a coalescence material even when the pore size is bigger than the droplet size. However, surface wettability and material thickness are important for coalescence to be effective. Contrary to membrane sieving, the surface of a coalescing material must have affinity to the dispersed phase, oil in our case, for it to be effectively separated. At the same time, the surface should not be too affinitive to oil in order for the oil droplets to be released with ease at a later time. There should exist a balanced point for ideal surface wettability, however, such wettability is difficult to define because pore size always comes into play. Pore size is relevant in determining the operating pressure; it affects

fluid dynamics and eventually separation efficiency. For a coalescing material, the pore size is typically bigger than the average droplet size for not only easy droplet release, but also small pressure differential across the material. Also because of the relative greater pore size as compared to a micro or ultra-filtration membrane, surface fouling and pore plugging of a coalescence material can be better mitigated. This feature makes coalescence advantageous over membrane sieving for treating emulsions 0.5-20 μm in size. Therefore, it is very important to quantify how surface wettability and pore size contribute to coalescence separation efficiency at the same time, provided other conditions such as material thickness, flow rate and emulsion size being the same. There are several reports defining non-woven material's relative surface wettability to oil and water and its effect on coalescence separation of water-in-oil emulsions,[50-52] but the effect of pore size was not taken into consideration. Regarding coalescence separation of oil-in-water emulsions, barely any work was published to reveal the co-effect of surface wettability and pore size of the coalescence material. This is interesting because coalescence is one of the major technologies used for oil-water separation in industries such as oil and gas exploration for produced water treatment, hydrometallurgical and pharmaceutical processes for expensive solvent recovery, and so on.

In this work, as a continuous effort of our previous research[49] exploring additional applications of commercial stainless steel felt, we studied in more details and depth the preparation of the material with various degrees of hierarchical structure and CVD coatings, to render the surface with dual roughness and dual liquid-phobicity, or

amphiphobicity. We challenged the coatings thus prepared for a much longer time to test the coating's durability in both soybean oil and acidic water. We measured the coating's thickness and tested the material's applicability for 4 emulsions, including hexadecane/water, octane/water, soybean oil/water and engine oil/water. Above all, using hexadecane/water emulsion as a model system, we made an effort to uncover the sensitivity of coalescence to surface wettability as well as pore size of the modified felt, in an attempt to provide more insights of coalescence separation, and answer the questions that have puzzled many people in this regard. In fact, the guidelines for designing effective coalescence materials are very fuzzy. Knowledge from past literatures is always conflicting because of the difficulty to separate the individual contribution of pore size and surface wettability, therefore their coupling effect as well. This is largely resulted from the inability to have the right porous materials as the subject of matter to study, which is achieved in the current work otherwise. The dual roughness formed by two size particles was designed to obtain a raspberry structure for the right surface wettability control for effective coalescence separation, which could not be easily accomplished by using single size particles.

2. Experimental section

2.1. Materials: 1H, 1H, 2H, 2H-perfluorooctyltriethoxysilane (POTS) and poly(dialkyldimethylammonium chloride) solution (PDDA, Mw = 200000–350000, 20 wt%) were obtained from Sigma Aldrich. The concentration of PDDA aqueous solution was fixed at 2 mg•mL^{-1} in all the experiments. Tetraethylorthosilicate (TEOS,

99+ %) was purchased from Alfa Aesar. Absolute ethanol (99.5%) and aqueous ammonia (25%) were obtained from Beihua Fine Chemicals Company. Monodispersed SiO_2 NPs of ca. 20 nm (S-20) and ca. 200 nm (S-200) were fabricated using Stöber method.[53] For the synthesis of 20 nm SiO_2 NPs, 3 ml TEOS were added dropwise to a flask containing100 ml absolute ethanol and 5 ml aqueous ammonia under magnetic stirring. The mixture was stirred at 60 ^oC for 17 hours. For the synthesis of 200 nm SiO_2 NPs, 3 ml TEOS were added dropwise to a stirred mixture of 100 ml absolute ethanol, 7.5 ml aqueous ammonia and 1 ml deionized water. The reaction lasted for 17 hours at room temperature. Noteworthily, the as-prepared suspensions of both 20 nm and 200 nm SiO_2 NPs had a pH value of ca. 10-11, and were used directly in the subsequent LBL self-assembling procedure. The sintered stainless steel fiber felts (filter precision: 5 μm) were purchased from Xinxiang Lier Filter Technology Co. Ltd., Xinxiang, China, and cut into circles 25 mm in diameter (SEM image shown in Figure S2 in Supporting Information). The pore size of the blank felt measured 10.0 μm as is shown in Figure S3 in supporting information. These fiber felts were used as substrates after repeated ultrasonication cleaning in deionized water and ethanol.

2.2. LBL Assembly of SiO_2 NPs: The cleaned fiber felts were immersed alternatively in PDDA solution (2 mg/mL) and the as-prepared suspensions of SiO_2 NPs (~0.1 wt. % estimated by chemical reaction stoichiometry) with varied particle size for 2 min. With both liquids being stirred constantly, we repeated the assembling cycles for a suitable number of times. Redundant polyelectrolytes (PDDA) or SiO_2 NPs in each

cycle were removed by hand-shaking the felt sample in pure water. Finally, a series of n+m SiO_2 NPs depositions were obtained on the felts after blow-drying with N_2 at room temperature. Here, n+m is used to denote n deposition cycles of 200 nm SiO_2 NPs and m deposition cycles of 20 nm SiO_2 NPs.

2.3. Hydrophobic Modification: The surface of the felt with SiO_2 NPs deposition was modified using simple CVD method. In a typical procedure, the felt was put into a Teflon container (100 mL) of a stainless steel autoclave, and varied amounts of POTS (volume: 5 or 50 μL) were dispensed to the bottom of the container. There existed no direct contact between the POTS solution and the substrate. Then the autoclave was sealed and placed in an oven pre-heated to 120 ^{o}C for 1 h to enable reaction between the vaporized POTS molecules and the hydroxyl groups on the substrate surface. Finally, the autoclave was cooled, opened and put in an oven for another 2 h at 150 ^{o}C to volatilize the unreacted POTS on the substrate.

2.4. Oil-Water Separation: To investigate the oil-water separation performance, the felts with and without particle deposition and CVD modification were used as oil droplet coalescers, the test setup for which is shown in Scheme 1. Blank commercial stainless steel felt was used as the control in all the experiments. A series of surfactant-free emulsions were prepared by mixing water and various oils (n-hexadecane, n-octane, soybean or engine oil) using a homogenizer (D-500, Wiggen Hauser, Germany) operating at 15000 rpm for 10 min. The initial oil concentration in the emulsion was 1000 mg/L. The droplet size of the emulsion was observed to be in the range of 1-20 μm using an optical microscopy. The average size was about 2-4 μm

and the emulsions stayed stable for 2 hours as reported in a separate research [54]. After it was prepared, the emulsion was immediately drawn into a syringe, and pushed through the felt mounted in a filter holder 25 mm in diameter with guaranteed seals. The separated oil floated to the top of the filtrate; the concentration of the un-separated oil in the filtrate was analyzed with the oil analyzer to determine the coalescence efficiency as described in our previous publication.[49]

2.5. Characterization: Freshly fabricated coatings were observed on a Hitachi S-6700 scanning electron microscope (SEM) operated at 10 kV. Water and oil contact angles (WCAs and OCAs) on different felt surfaces were measured at ambient temperature by using a contact angle/interface system (OCA-20, Dataphysic), where 4 μL liquid volume was employed for proper observation unless otherwise indicated. X-ray photoelectron spectroscopy (XPS) analysis of the coating components was conducted using an ESCALAB 250 Xi system of Thermo Fisher Scientific. Quantachrome Porometer 3G through-pore size analyzer was used to measure the pore size. The oil-in-water emulsion size was observed with an optical microscopy (6XB-PC) made by Shanghai optical instrument factory. Droplet volume size distribution was measured using a Beckman-Coulter laser diffraction particle size analyzer (LS13320). The oil content in water was determined with an Oil 460 infrared photometer oil content analyzer from the Beijing China Invent Instrument Tech. Co. Ltd., Beijing, China. Inductively coupled plasma–optical emission spectrometer (ICP–OES) from Thermo Scientific (ICAP-5300DV) was used at wavelength of 251.611 nm to determine the possible existence of Si in ultrasonicated solutions

immersed with and without the coated felt. This was to check if coatings came off from the substrate under severe challenging conditions, an indirect way to test coating adhesion. Thermogravimetric analysis (TGA) was conducted on a simultaneous DSC-TGA analyzer (SDT Q600, TA Instruments).

3. Results and discussion

3.1. Self-assembly of Hierarchical Rough SiO_2 NPs Deposition Followed by Hydrophobic Modification

The substrate surface of stainless steel fiber felt was structured with 200 nm and 20 nm SiO_2 NPs by LBL self-assembly. With the help of the deposited PDDA layer which is positive charged, the SiO_2 NPs with negative charges were assembled on the fiber surface by electrostatic interaction. The SEM images in Figure 1 show the morphologies of the felt surfaces with n+m deposition cycles of PDDA/SiO_2 NPs. Here again n+m is used to denote n deposition cycles of 200 nm SiO_2 NPs and m deposition cycles of 20 nm SiO_2 NPs. As shown in Figure 1a, SiO_2 NPs were assembled successfully as a uniform single particle layer on the fiber surface. In order to construct hierarchically roughened surface, we deposited 200 nm SiO_2 NPs on the fibers a few times first, and then assembled the 20 nm SiO_2 NPs on the surface just once. The morphologies of such surfaces are shown in Figure 1b-d. It was observed that the bigger particles were not deposited as a dense layer, which might be caused by their large size that intervened with electrostatic adsorption. The number of bigger particles increased on the surface when the corresponding deposition cycles were increased. When four deposition cycles of 200 nm SiO_2 NPs plus one deposition of 20

nm SiO_2 NPs were applied, relatively uniform, raspberry-like single particle layer was formed nicely on the felt surface (Figure 1d). In addition, as shown in Figure S4 (Supporting Information), with lower-magnification SEM imaging of the corresponding fiber felts, it was found that after LBL assembly, the pores of the felt were still open, the crossing fibers were covered with merely nano-scaled assemblies that could barely be distinguished by naked eyes in these images.

The blank stainless steel fiber felt and felts with 0+1, 1+1, 2+1, and 4+1 particle depositions were further treated hydrophobically with CVD. To study the different levels of chemical coating effect (related to coating coverage that affects surface energy of the felt), we applied 5 μL and 50 μL POTS in the autoclave respectively for the treatment. As shown in Figure S5 in the Supporting Information, treatment with neither high nor low amount of POTS affected the surface morphology of the particle depositions. Actually, comparing the original assembly of 1+1 deposition (Figure 1b and Figure S4b) with what is shown in Figure S5, it is reasonable to think that the hydrophobic modification must be a very thin POTS layer, so that the hierarchical structure of the felt is retained. We further conducted energy dispersive X-ray spectrometry (EDXS) analysis to the POTS coatings, and Figure S6 in the Supporting Information shows the results. The felt with 1+1 particle depositions plus CVD treatment using the higher amount of POTS showed 2.4 wt% presence of fluoride. No fluoride was detected for the felt treated with the lower amount of POTS, possibly due to (1) the low detection limit (0.1 wt%) of EDXS at our experimental condition of 15kV, (2) the deep detection depth of EDXS that goes beyond the thickness of the

coating, which leads to underestimation of the fluoride content when averaged across the detection depth. XPS was then used to analyze the kinds of chemicals on the surfaces, and the result is presented in Figure 2. The atomic fraction ratio F:Si on the surfaces treated with the high and the low amount of POTS is 92.8:7.2 and 81.3:18.8, respectively. This is a clear indication that more F-containing components were deposited on the felt surface when the initial amount of the fluorosilane used was higher. Moreover, as shown in Figure S7 in the Supporting information, the atomic fraction ratio F:Si of POTS is 13:1. During CVD modification, POTS reacted with silanol groups on the surface of SiO_2 NPs to form –O-Si-O– covalent bond, and individual ethanol molecules formed were removed, thus the atomic fraction ratio of F and Si of the formed fluorosilane layer ought to still be 13:1 (See Figure S8 for the detailed reaction mechanism in Supporting information). The ratio measured for the surface treated with the lower amount of POTS is 4.3:1(81.3:18.8), much smaller than the theoretical ratio. That is because the CVD coating layer is thinner than the XPS detection thickness (around 10 nm), so SiO_2 NPs under the coating is reached, causing an over-calculation of Si, therefore under-calculation of F in the chemical deposition layer. Interestingly, the F:Si ratio in the CVD deposition layer treated with the higher amount of POTS is very close to that of POTS itself (92.8:7.2=12.9:1≈13:1), indicating the deposition layer is close to a thickness of 10 nm.

3.2. Pore Size and Wetting Properties

Figure 3 summarizes the pore size distribution of the blank stainless steel fiber felt, and the felts assembled with 0+1, 1+1, 2+1 and 4+1 particles coatings. All the

felts were CVD treated in the autoclave using 5 μL POTS for surface liquid repellency. The mean pore size ranks in the order of 9.9 μm, 9.2 μm, 8.8 μm, 8.0 μm and 7.4 μm. As expected, the pore size becomes smaller with more particle depositions on the fiber surface. The stainless steel fiber size is around 10 μm, the larger SiO_2 particle used for LBL assembling is 200 nm, and the smaller SiO_2 particle is 20 nm. Since the CVD coating layer on the particle deposited felt is estimated to be thinner than 10 nm as discussed earlier, so it won't affect the pore size much. Apparently, the reduction in mean pore size is a result of particle deposition, and the size can be controlled by the number of particle deposition cycles via LBL assembly. Table 1 lists all the WCAs and OCAs on the various felts prepared above. The volume of the liquid droplet used for contact angle measurement is 4μL. WCA of the clean stainless steel fiber felt without any treatment is 80 ± 1^{o}. As shown in this table, the hydrophobic modification decreases the surface energy of the stainless steel felt, WCA increases to $136^{o}\pm1^{o}$ with the low level CVD treatment and 146 ± 1^{o} with the high level CVD treatment using POTS. TG analysis under air atmosphere of the coated felts showed 8 times instead of 10 times reacted POTS in the high level CVD case that of the low level case, indicating not all the POTS had reacted. However, the amount of POTS reacted does not proportionally correlate to WCA when there are already enough POTS molecules on the surface, a typical surface phenomenon that explains the only 10º WCA difference for the two levels of CVD treatment. As expected, no matter what level of the chemical treatment was applied, WCA on the coated surfaces increased step by step with increasing nanoparticle deposition cycles due to the increased

surface roughness. However, the surface with the low level CVD treatment could not reach super-hydrophobicity that required WCA to be equal to and greater than 150°. This may be because, as Wenzel theory[55] indicates ($\cos\theta' = r\cos\theta$), the surface energy of the treated SiO_2 is not low enough to trap air and prevent water from penetrating into the inner surfaces of the hierarchical structure. As discussed earlier, more F-containing component reacted with SiO_2 particles when the higher amount of POTS (50 μL) was used during CVD treatment, resulting in a WCA as high as 158 $\pm 1^{o}$ on the surface with 4+1 nanoparticle deposition. On the contrary, the WCA on the same particle-roughened surface further treated with the lower amount of POTS (5μL) is only 147 ± 1^{o}. The wetting behavior in the former case suits Cassie wetting model[56] ($\cos\theta' = f\cos\theta + f - 1$), where water droplet cannot easily adhere to this superhydrophobic surface (see video in the Supporting Information). It indicates again that the hierarchically structured surface (sharp roughness due to particle deposition) and the low enough surface energy (due to CVD treatment with sufficient amounts of POTS) are both essential for constructing a superhydrophobic surface. Because the CVD treatment agent POTS is a fluorosilane, the surfaces become not only hydrophobic but also oleophobic, or rather amphiphobic. As shown in Table 1, OCA (n-hexadecane as the oil) on each surface follows the same trend of WCA.

3.3. Oil-Water Separation

The felts prepared in this work were designed as oil coalescence materials. To conduct the separation experiments, 50 ml 1000 mg/L oil-in-water emulsion were forced through the felt in 60 seconds with constant speed as demonstrated in Figure 4.

The pressure differential across the felt was lower than 5 kPa. Small oil droplets in water were captured, enlarged and released from the felt, floating to the top of the filtrate as separated oil. Unseparated oil in the bulk of the filtrate, if any, was analyzed to determine its concentration by the oil content analyzer mentioned earlier. Figure 4 (b) & (c) are illustrative optical photographs of an exemplar octane-in-water emulsion before and after filtration. The oil-water emulsion separation efficiency was calculated using Equation 1:

$$R_o=(1-C_p/C_0)*100\% \quad (1)$$

Where C_p is the oil concentration in the filtrate, C_0 is the feed oil concentration. The oil concentration unit used is mg/L. The hexadecane-water emulsion separation efficiency of the bare felt as control was found to be only 28% as reported in our previous work.[49] The efficiency of the felts CVD-treated only with the low and the high amounts of POTS is 95% and 75%, respectively, much higher than that of the bare felt, signifying the importance of surface water repellency for oil coalescence. However, if the surface water repellency is too high, it negatively effects on separation. Here, the two felts without any particle deposition have similar pore size, but the more hydrophobic (WCA is 146 ± 1^{o} vs. 136 ± 1^{o}) and oleophobic (OCA is 107 ± 2.7^{o} vs. 94 ± 1^{o}) felt is less efficient for separation. Calculation of the underwater oil contact angle on these felts using the underwater wetting theory[48,57] showed different results, with the lightly-treated felt being 20^{o}, and the heavily treated one 4^{o}. The higher underwater oil contact angle in this case gave better separation. The explanation of the result has to go back to coalescence mechanism. If the surface is

too affinitive for oil under water (the more water repellent surface in air), the felt will be much more easily wetted by oil. By capillary forces, an oil film will form inside the material that adds resistance to flow. And at a certain point, the film bulges under flow shear, then explodes and breaks into fine droplets, which are carried away by water flow to downstream, resulting in bad separation. But when looking at the felts with both chemical and particle deposition, we found no correlation between the calculated underwater oil contact angle and the separation efficiency, no matter what level of chemical treatment was applied to the felt of similar pore size. What this implies is that the applicability of such theory to the roughened surface is not appropriate here. In fact, when we forced an oil droplet to be in contact with these roughened materials under water, the droplet quickly spread and made its way into the felts. It indicates that the felts are wettable by oil underwater but the speed of wetting is very difficult to quantify experimentally and theoretically. A static contact angle characterization underwater is therefore less meaningful although observationally helpful. Realizing that, we had to go back to the surface wetting or non-wetting behavior in air because these surfaces were made both hydrophobic and oleophobic, static water and oil contact angle on them stayed unchanged for tens of minutes, thus comparison of the measured data made good sense. Table 1 summarizes all the data including pore size and separation efficiency. As it shows, the felt with 4+1 particle deposition has the highest efficiency regardless of the levels of CVD treatment with POTS. However, considering the experimental error for efficiency determination, pore size does not appear to affect the separation efficiency when the surface is less

amphiphobic due to the lighter CVD treatment. On the contrary, when the surface is more amphiphobic with heavier CVD treatment, decreased pore size leads to increased efficiency. More importantly, at the same pore size, less amphiphobic surface gives higher separation efficiency. This is true for each pair of the felts with the same cycles of particle deposition but different levels of CVD treatment. To make the observation more straightforward, a histogram is plotted and shown in Figure 5, and further information can be found in Figure S9 in the Supporting Information with the efficiency and contact angle data being plotted together.

To test the separation capacity of the treated felt for different oil-in-water emulsions, 1000 mg/L n-octane-in-H_2O, soybean oil-in-H_2O and engine oil-in-H_2O emulsions were also prepared using the same procedure. 50 ml of each emulsion was then filtered in a single flow pass with the felt having 2+1 particle deposition plus the low level CVD hydrophobic modification. The results are shown in Figure 6. The separation efficiency of soybean oil/water emulsion was 99%, the highest. That of N-hexadecane/water and n-octane/water was all above 95%. The lowest separation occurred to the engine/water emulsion, which was only 90%. Optical microscopic observation showed an average size of 2-4 μm for all the emulsions stable for about 2 hours. The lowest efficiency for engine oil/water is possibly due to the highest viscosity of the oil among others (3 times that of soybean oil[54]),which causes reduced oil droplet mobility and collision for confluence. The other reason could be that the engine oil has surface active additives that interfere with the coalescence separation.

To study the stability of the surface coating prepared in this work, we repeatedly

used the felt with 2+1 particle deposition and the lower level CVD treatment for 20 times for filtration of n-hexadecane/water emulsion. After each filtration, the felt was washed and rinsed with deionized water and dried before the next use. It was found the filtration efficiency only dropped by 0.2%, which is a good indication of the coating's short-term stability and durability.

To test the felt's long time reproducibility for separation, we stored the used felt (used for 20 times for filtration of n-hexadecane/water emulsion) for one and five months, and then used it again for separating the emulsion. The filtration efficiency now dropped from 99% to 97% and 97% respectively as shown in Figure 7. The slight decrease in efficiency, although a concern to some extent, is indicative of the relatively good reproducibility of the coated material. In fact, using PDDA as the binder, SiO_2 nanoparticles as the building blocks and a fluorosurfactant as a modifier, a recent research conducted by Brown et al, also demonstrated the similar stability of LBL coatings on stainless steel mesh and glass plate respectively.[58]

To further test the coating's long-term durability, we decorated a stainless steel mesh with the same coating as for the felt, and challenged the mesh in oil and acid solution by immersing it in these liquids for about 8 months. The open mesh structure allowed the coating to be more exposed to the liquids as compared to the tight felt. We then took the mesh sample out of the liquids from time to time, cleaned it with isopropanol and deionized water, dried it in air, and measured the WCAs on its surface. The result is shown in Figure 8. The WCA stayed unchanged after the first 5-day immersion in both the oil and the acid solution; after 8 months, it decreased

from 158±1° to 135±1° and 135±1° respectively in oil and the acidic water. This indicates the coating is relatively intact. However, further improvement may still be needed if much longer term application is expected.

The coalescence experiments carried out in this work merit further discussion in order for the method to be universally applicable. This is a method we designed in our own lab for its speed and simplicity to test emulsion separation efficiency of a coalescence material. The narrow neck of the syringe has an inner diameter of 1.5 mm and measures 13 mm long. It was suspectable to cause some shear-induced coalescence of the emulsion passing through it, although the emulsion itself stayed stable for hours and the coalescence experiment took only 60 seconds to finish. To examine the possible side effect of the neck, we measured the volume size distribution of the original hexadecane-in-water emulsion, the emulsion going through the syringe only, and the emulsion going through the whole coalescence setup with the coated filter (2+1) in it. The result is given in Figure S10 in the Supporting Information. As it shows, this narrow neck did slightly change the drop size distribution. Indeed, a very small fraction of the drops was squeezed to coalesce in the neck because of fluid shear. The coalesced drop size ranged from 50 to 100 μm, but the majority of the drops retained their original size ranging 0.5-20 μm. The majority of the separation was certainly attributed to the coated felt as strongly indicated by the drop size distribution after the emulsion passed through the felt. The major size of the drops shifted to 30-500 μm, with a small fraction still sitting in the range of 0.5-2.5 μm, escaping the separation. This indicates the experimental method is sound but improvement can still

be made by enlarging the neck.

Coating adhesion is a common concern for any type of coating technology. Although it was strongly evidenced that our nano-coating was robust and durable subject to regular flow shear during experiments, would it survive severe shaking or vibration? To check on this, we put the coated felt into deionized (DI) water and ultrasonicated it for 1h (work power is 270W). This was to find out if any coatings would fall off from the felt in such harsh conditions. We then measured Si content in the water using ICP-OES and compared it with that in 20 ml pure DI water. We also put another piece of the coated felt of the same mass in 20 ml 2M NaOH solution and applied the same amount of sonication to strip off total SiO_2 from the felt and measured it accordingly. The result is given in Table S1 in supporting information. As can be seen, the amount of Si coming off from the felt is out of ICP detection limit of 0.014 ppm, and the data falls in the same order of magnitude of pure DI water. This means very likely, extremely small amount of SiO_2, if any, came off. The total amount of SiO_2 coating on the felt is 2.3 ppm as also shown in the table. Regardless of the accuracy of the detection for the extreme small concentrations of Si, the highest possible amount of SiO_2 shed from the coated fiber felt under ultrasonication is merely 0.3%, proving good adhesion between the particles and the substrate.

Finally, a question need to be asked as to whether there is any relevance of macroscopically measured contact angles to microscopic phenomena that take place in the felt during oil-in-water emulsion separation. For contact angle using both water and oil as the probing liquids, we followed the typical protocol proposed.[59] The

volume of the liquid is 4 μL, corresponding to about 2 mm diameter, 8000 times the dimension of the assembled particles and the spacing among them to accommodate the imperfection of the surface.

There are three aspects to elaborate for answering the question. First, the measurement of contact angle using different size probing liquid will bring some difference to the results. Large droplet tends to distort the shape of the liquid sitting on a surface to give a lower contact angle in air. It also helps to spread the droplet more quickly if the surface is wettable. However, the general trend of the measurement using both small and big droplets should be not affected on a flat surface. On the other hand, if the surface is not perfect or full of peaks and valleys, than the use of big droplet is preferred. Now will the measurement relate to the measurement using small droplet? It should if the small droplet is still much bigger than the roughness characteristic dimension. There may not be correlation if the droplet size is in the same dimension range of the roughness, because the droplet can well be either on the top of a few peaks, or in the valleys of the surface, which will give different results. But again this all refers to the measurement in air.

Second, let's consider in a filtration process how the droplets interact with the felt. Droplets smaller than the pore size will be captured via interception or diffusion mechanism by the felt fibers, large droplets will impact with the material surface right away and be forced to deform. After being captured, small droplets wet out the surface typically without strong external forces, but large droplets will be forced to wet the fiber surface by hydrodynamic shear stress. So there is a difference here in

terms of the force the droplets are subject to, but the physical nature of the wetting should not differ. During a coalescence process, small droplets will join force with the large droplets to form a thin film around the fiber, and the thickness of the film will grow until it cannot hold itself together to form big suspended droplets, which will be swept away and merge with other droplets to grow even bigger for separation. The whole process involves droplet capture, droplet wetting, droplet growth and droplet release. The felt surface wetting by the small droplets under water, which is determined by its wetting with both oil and water in air, plus oil-water interfacial tension, becomes significant at the beginning and the middle of the separation process inside the coalescing material. Droplets in millimeter size will typically appear at the downstream side of the material, where they have to overcome the capillary force for release, leaving behind possibly a small residue on the material surface. But again the inherent wetting trend by both the big droplets and the small droplets is the same in nature regardless of the possible experimental difference in apparent contact angle measurement.

Third, will the small droplet stay on the fiber surface when it hits the surface in the first place? This has much to do with the adhesion between the droplet and the fiber surface. In its essence, the adhesion induced by molecular forces is the same for both big and small droplets in nature. The only difference is the droplet stability on the surface, big droplet tends to be less stable subject to high shear stress if the surface is not immediately wettable underwater. If the surface is immediately wettable, this is less a problem. Nonetheless, all these happen under dynamic flow conditions and

static contact angle measurement cannot address them alone, irrelevant to the droplet size used for contact angle measurement.

Overall, the interaction of droplets with the felt is different for big droplet size (bigger than pore size) than small size droplets for droplet capturing. The adhesion of both size droplets on the surface is not significantly different in nature, so the use of big droplet for contact angle measurement in air should relate to the underlying behavior of the small droplets underwater during filtration. However, it is understood the interaction of the droplets with the felt under flow is way more complex than said, which merits fundamental studies in the future.

4. Conclusions

Stainless steel fiber felts with hierarchical surface structure formed by SiO_2 NPs deposition via LBL self-assembly were successfully fabricated and further hydrophobically treated using CVD. These modified felts can effectively separate various 3 μm oil-in-water emulsions by coalescence with the highest separation occurred to soybean/water emulsion. The effect of the felts' surface wettability and pore size on coalescence separation efficiency was carefully studied using n-hexadecane/water emulsion as a model system. It was discovered the first time that when the surface of the material was less amphiphobic, smaller pore did not affected much the separation. However, when the surface was more amphiphobic, the separation was interestingly more sensitive to the change of pore size, with smaller pores giving higher efficiencies. When pore size was kept the same, then less

amphiphobic surface was preferred to leverage the separation. The findings in this work are expected to provide better guidelines for designing coalescence materials, where a material's surface property always intermingles with its pore size tailoring.

Acknowledgements

This work was supported by the Chinese Academy of Sciences under the talented program, and by the National Natural Science Foundation of China (Grant number 21401201 and 21476237).

Notes and references

1 B. Wang, W. Liang, Z. Guo and W. Liu, *Chem. Soc. Rev.* 2015, **44**, 336-361.

2 A. Fakhru'l-Razi, A. Pendashteh, L. C. Abdullah, D. R. A. Biak, S. S. Madaeni and Z. Z. Abidin, *J. Hazard. Mater.* 2009, **170**, 530-551.

3 Z. Xue, Y. Cao, N. Liu, L. Feng and L. Jiang, *J. Mater. Chem. A* 2014, **2**, 2445-2460.

4 M. Santander, R. T. Rodrigues and J. Rubio, *Colloids Surf., A* 2011, **375**, 237-244.

5 P. C. Chen and Z. K. Xu, *Sci. Rep.* 2013, **3**, 2776.

6 D. Angelova, I. Uzunov, S. Uzunova, A. Gigova and L. Minchev, *Chem. Eng. J.* 2011, **172**, 306-311.

7 T. R. Annunciado, T. H. Sydenstricker and S. C. Amico, *Mar. Pollut. Bull.* 2005, **50**, 1340-1346.

8 A. K. Kota, G. Kwon, W. Choi, J. M. Mabry and A. Tuteja, *Nat. Commun.* 2012, **3**, 1025.

9 L. Zhang, Y. Zhong, D. Cha and P. Wang, *Sci.Rep.* 2013, **3**, 2326.

10 L. Wu, J. P. Zhang, B. C. Li and A. Q. Wang, *J. Mater. Chem. B* 2013, **1**, 4756-4763.

11 B. Wang and Z. Guo, *Chem. Commun.* 2013, **49**, 9416-9418.

12 X. Zhou, Z. Zhang, X. Xu, F. Guo, X. Zhu, X. Men and B. Ge, *ACS Appl. Mater. Interfaces* 2013, **5**, 7208-7214.

13 B. Cortese, D. Caschera, F. Federici, G. M. Ingo and G. Gigli, *J. Mater. Chem. A* 2014, **2**, 6781-6789.

14 Y. Cao, N. Liu, C. Fu, K. Li, L. Tao, L. Feng and Y. Wei, *ACS Appl. Mater. Interfaces* 2014, **6**, 2026-2030.

15 M. M. Pendergast and E. M. V. Hoek, *Energy Environ. Sci.* 2011, **4**, 1946-1971.

16 W. Zhang, Y. Zhu, X. Liu, D. Wang, J. Li, L. Jiang and J. Jin, *Angew. Chem. Int. Edit.* 2014, **53**, 856-860.

17 Z. Shi, W. B. Zhang, F. Zhang, X. Liu, D. Wang, J. Jin and L. Jiang, *Adv. Mater.* 2013, **25**, 2422-2427.

18 W. Zhang, Z. Shi, F. Zhang, X. Liu, J. Jin and L. Jiang, *Adv. Mater.* 2013, **25**, 2071-2076.

19 Y. Zhu, F. Zhang,; D. Wang, X. F. Pei, W. Zhang and J. Jin, *J. Mater. Chem. A* 2013, **1**, 5758-5765.

20 H. C. Yang, J. K. Pi, K. J. Liao, H. Huang, Q. Y. Wu, X. J. Huang and Z. K. Xu, *ACS Appl. Mater. Interfaces* 2014, **6**, 12566-12572.

21 Y. Xiang,; Liu, F.; Xue, L. *J. Membr. Sci.* 2015, **476**, 321-329.

22 Y. Liu, Y. Su, Y. Li, X. Zhao and Z. Jiang, *RSC Advances* 2015, **5**, 21349-21359.

23 H. W. Kim, H. D. Lee, S. J. Jang and H. B. Park, *J. Appl. Polym. Sci.* 2015, **132**, 41661.

24 D. Wandera, H. H. Himstedt, M. Marroquin, S. R. Wickramasinghe and S. M. Husson, *J. Membr. Sci.* 2012, **403**, 250-260.

25 L. Wen, Y. Tian, J. Ma, J. Zhai and L. Jiang, *Phys. Chem. Chem. Phys.* 2012, **14**, 4027-4042.

26 X. Yao, Y. Song and L. Jiang, *Adv. Mater.* 2011, **23**, 719-734.

27 X. Li and J. He, *ACS Appl. Mater. Interfaces* 2013, **5**, 5282-5290.

28 X. Du, X. Li and J. He, *ACS Appl. Mater. Interfaces* 2010, **2**, 2365-2372.

29 Z. Cheng, H. Lai, Y. Du, K. Fu, R. Hou, C. Li, N. Zhang and K. Sun, *ACS Appl. Mater. Interfaces* 2013, **6**, 636-641.

30 M. Jin, S. Li, J. Wang, Z. Xue, M. Liao and S. Wang, *Chem. Commun.* 2012, **48**, 11745-11747.

31 X. T. Zhu, Z. Z. Zhang, X. H. Xu, X. H. Men, J. Yang, X. Y. Zhou and Q. J. Xue, *J. Colloid Interface Sci.* 2012, **367**, 443-449.

32 J. Zhang, A. Wang, S. Seeger, *Adv. Funct. Mater.* 2014, **24**, 1074-1080.

33 Z. Chu, Y. Feng, S. Seeger, *Angew. Chem. Int. Edit.* 2015, **54**, 2328-2338.

34 Z. Xue, Z. Sun, Y. Cao, Y. Chen, L. Tao, K. Li, L. Feng, Q. Fu and Y. Wei, *RSC Adv.* 2013, **3**, 23432-23437.

35 J. Zhu, H. Li, J. Du, W. Ren, P. Guo, S. Xu and J. Wang, *J. Appl. Polym. Sci.* 2015, **132**, 41949.

36 C. R. Gao, Z. X. Sun, K. Li, Y. N. Chen, Y. Z. Cao, S. Y. Zhang and L. Feng, *Energy Environ. Sci.* 2013, **6**, 1147-1151.

37 Z. Xue, S. Wang, L. Lin, L. Chen, M. Liu, L. Feng, L. Jiang, *Adv. Mater.* 2011, **23**, 4270-4273.

38 J. Song, S. Huang, Y. Lu, X. Bu, J. E. Mates, A. Ghosh, R. Ganguly, C. J. Carmalt, I. P. Parkin, W. Xu and C. M. Megaridis, *ACS Appl. Mater. Interfaces* 2014, **6**, 19858-19865.

39 C. H. Lee, N. Johnson, J. Drelich, Y. K. Yap, *Carbon* 2011, **49**,669-676.

40 B. Ge, Z. Zhang, X. Zhu, X. Men, X. Zhou, *Colloids Surf., A* 2014, **457**, 397-401.

41 Y. Huang, C. Li and Z. Lin, *ACS Appl. Mater. Interfaces* 2014, **6**, 19766-19773.

42 L. Peng, S. Yuan, G. Yan, P. Yu and Y. B. Luo, *J. Appl. Polym. Sci.* 2014, **131**, 40886.

43 A. Li, H.-X. Sun, D.-Z. Tan, W.-J. Fan, S.-H. Wen, X.-J. Qing, G.-X. Li, S.-Y. Li and W.-Q. Deng, *Energy Environ. Sci.* 2011, **4**, 2062-2065.

44 D. Wu, Z. Yu, W. Wu, L. Fang and H. Zhu, *RSC Adv.* 2014, **4**, 53514-53519.

45 L. Wu, L. Li, B. Li, J. Zhang and A. Wang, *ACS Appl. Mater. Interfaces* 2015, **7**, 4936-4946.

46 Q. An, Y. Zhang, K. Lv, X. Luan, Q. Zhang and F. Shi, *Nanoscale* 2015, **7**, 4553-4558.

47 Q. Liu, A. A. Patel and L. Liu, *ACS Appl. Mater. Interfaces* 2014, **6**, 8996-9003.

48 X. Zheng, Z. Guo, D. Tian, X. Zhang, W. Li and L. Jiang, *ACS Appl. Mater. Interfaces* 2015, **7**, 4336-4343.

49 X. Li, D. Hu, K. Huang and C.Yang, *J. Mater. Chem. A* 2014, **2**, 11830-11838.

50 P. S. Kulkarni, S. U. Patel and G. G. Chase, *Sep. Purif. Technol.* 2014, **124,** 1-8.

51 S. U. Patel and G. G. Chase, *Sep. Purif. Technol.* 2014, **126**, 62-68.

52 P. S. Kulkarni, S. U. Patel and G. G. Chase, *Sep .Purif. Technol.* 2012, **85**, 157-164.

53 W. Stöber, A. Fink and E. Bohn, *J. Colloid Interface Sci.* 1968, **26**, 62-69.

54 D. Hu, X Li, L Li and C. Yang, *Sep. Purif. Technol.*2015, **149**, 65-73
55 R. N. Wenzel, *Ind. Eng. Chem.* 1936, **28**, 988-994.
56 J. Bico, C. Tordeux and D. Quéré, *EPL- Europhys. Lett.* 2001, **55**, 214-220.
57 B. Bhushan,; Y. C. Jung and K. Koch, *Langmuir* 2009, **25**, 3240-3248.
58 P. S. Brown and B. Bhushan, *Sci. Rep.* 2015, **5**, 8701.
59 J. Drelich, *Surface Innovations,* 2013*,* **1**, 248-254

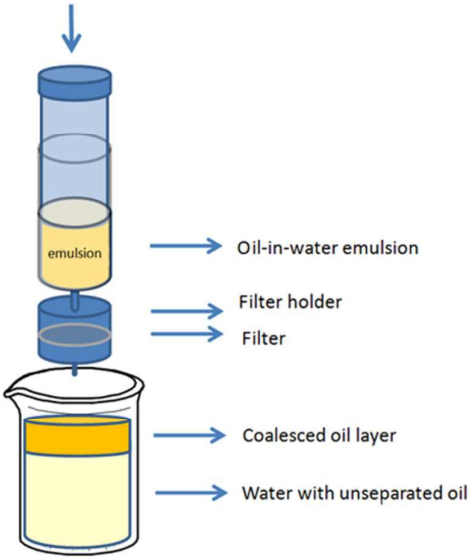

Scheme 1. Schematic diagram of the filtration system for oil-water emulsion separation.

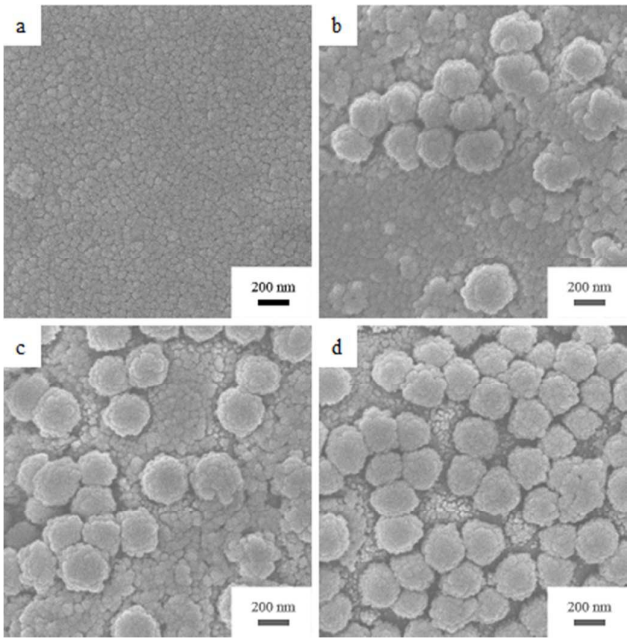

Figure 1. SEM images of stainless steel fiber felt with particle deposition obtained by (a) 0+1, (b) 1+1, (c) 2+1 and (d) 4+1 cycles of assembling before hydrophobic modification (n+m is used to denote n deposition cycles of 200 nm nanoparticles and m deposition cycles of 20 nm SiO_2 nanoparticles bilayer).

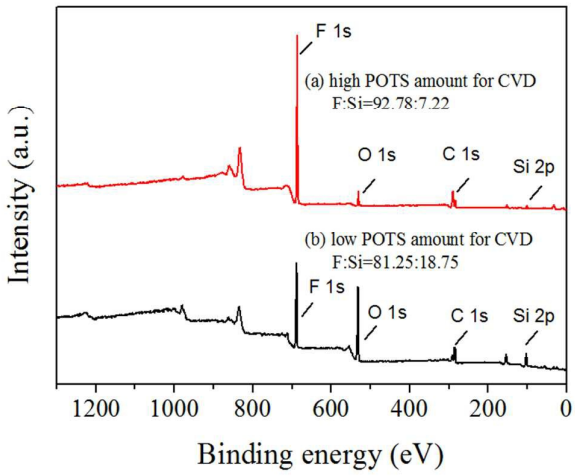

Figure 2. XPS spectrum of the felt coated with both particles and (a) high amount of POTS, and (b) low amount of POTS.

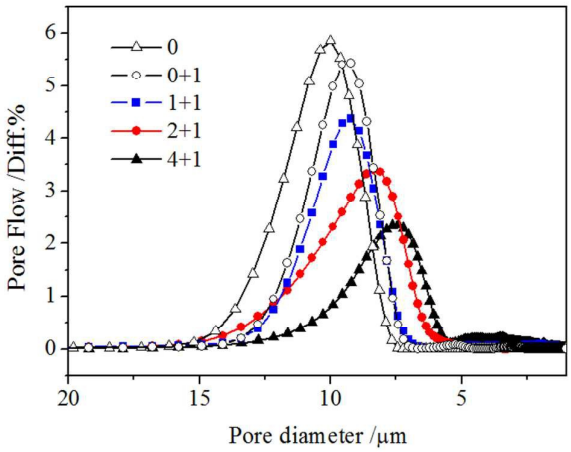

Figure 3. Pore size distribution of blank stainless steel fiber felt (0), felts with 0+1, 1+1, 2+1 and 4+1 particle depositions and CVD coatings with low amount of POTS.

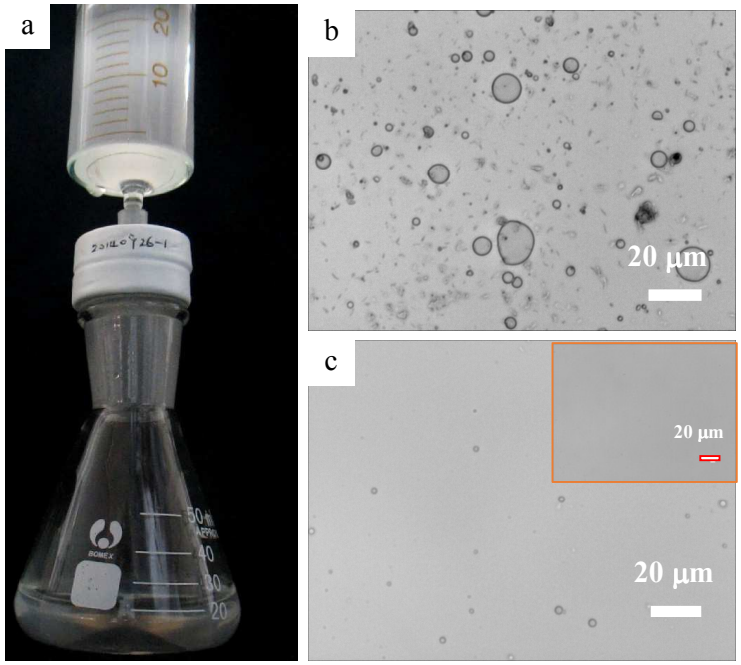

Figure 4. The optical photograph of (a) the octane-in-water emulsion separation process, emulsions (b) before and (c) after coalescence separation, inset is a picture from a different area showing no droplets remaining, scale bar is 20 µm.

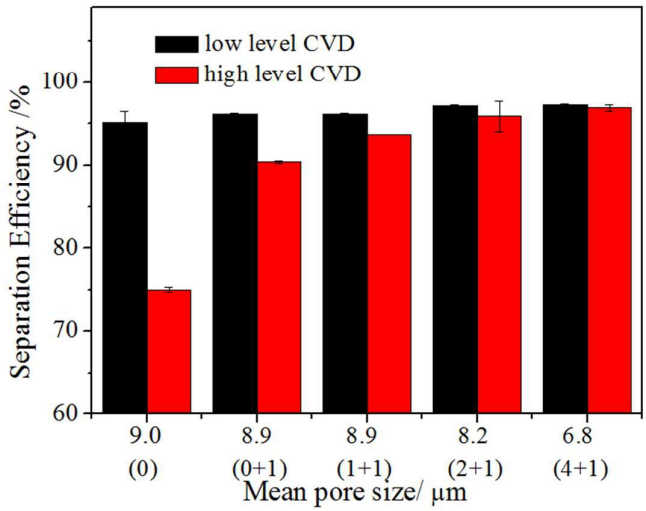

Figure 5. Separation efficiency vs. felts endowed with various properties.

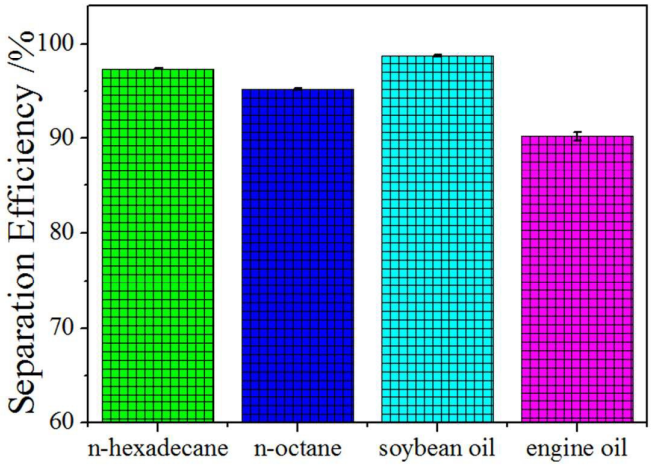

Figure 6. Separation efficiency for various oil-in-water emulsions filtered by the felt with 2+1 particle deposition and the low level CVD treatment with POTS.

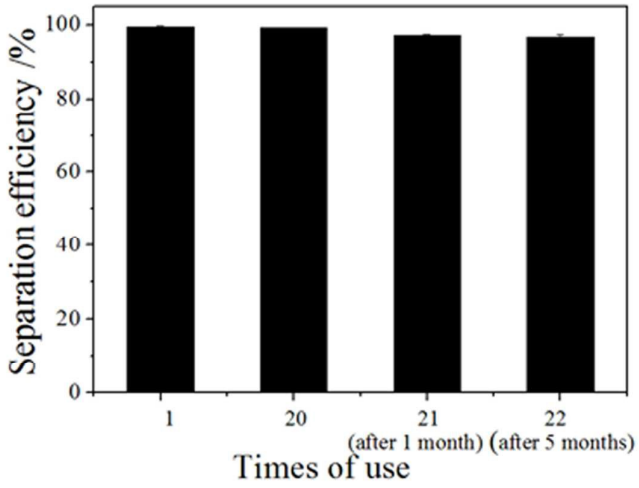

Figure 7. Separation efficiency and long-time reproducibility performance of hydrophobic particle-coated felt for n-hexadecane-in-water emulsion.

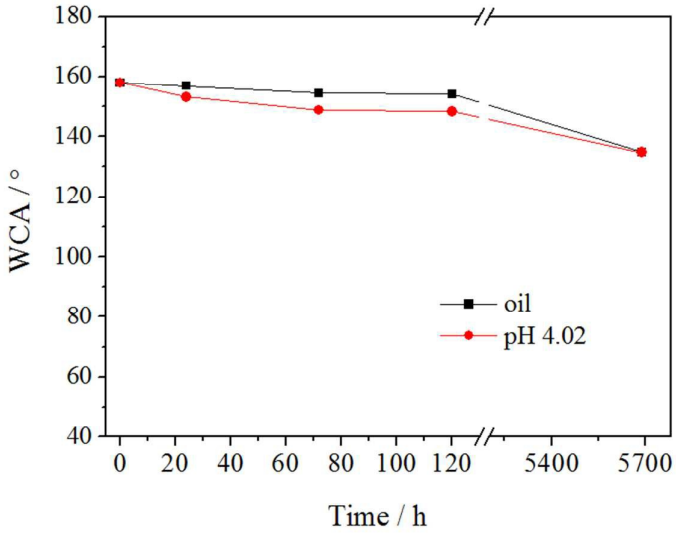

Figure 8. Change in WCA vs. time on the modified mesh immersed in soybean oil and hydrochloric acid solution (pH 4.02) respectively for continuous 8 months.

Table 1. Summary of felt properties and separation efficiencies of n-hexadecane-water emulsion. All the data are an average of three experiments. The initial oil concentration of the emulsion is 1000 mg/L.

Felt features	0	0+1	1+1	2+1	4+1
WCA of FPLC [a]	136±1	143±1	145±2	145±1	147±1
OCA of FPLC [a]	94±1	110±1	104±3	102±2	128±1
Oil-water separation efficiency of FPLC [a]	95%	96%	96%	97%	97%
WCA of FPHC [b]	146±1	144±2	153±1	157±1	158±1
OCA of FPHC [b]	107±3	120±1	126±1	130±1	133±1
Oil-water separation efficiency of FPHC [b]	75%	90%	94%	96%	97%

[a] FPLC is short for felt with particle deposition and low level CVD treatment.

[b] FPHC is short for felt with particle deposition and high level CVD treatment.

Table of Contents Graphic

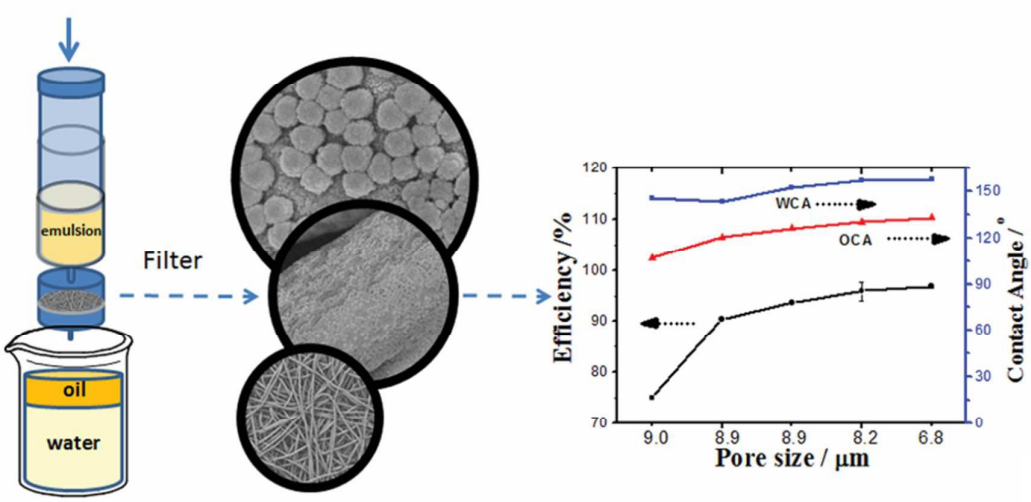

Coalescence sensitivity to surface wettability and pore size of roughened stainless steel felt was revealed for oil-in-water emulsion separation